Fabrication of carboxylic functionalized poly(methacrylic acid 2-(tert-butylamino)ethyl ester)-coated mesoporous silica nanoparticles and their application for removing ionic dyes from polluted water

Abdullah Mohammed Alswieleh

Department of Chemistry, College of Science, King Saud University, Riyadh, Kingdom of Saudi Arabia

ARTICLE INFO

ABSTRACT

The removal of dyes from wastewater that are released during industrial processes has become a significant concern in the environmental science in recent years. To tackle this issue, researchers are exploring the use of nanomaterials for designing new adsorbents. Another promising approach is to grow polymer brushes with high density functional groups via surface-initiated atom transfer radical polymerization (SI-ATRP), which can significantly enhance their ability to absorb dyes. The presence of carboxylic acid groups on the adsorbent material significantly contributes to its efficacy in dye removal by enhancing adsorption capacity, enabling selective adsorption, pH-dependent behavior, chelation, or complexation, and providing stability for repeated usage. In this work, a nanomaterial of carboxylic functionalized poly (methacrylic acid 2-(tert-butylamino)ethyl ester)-coated mesoporous silica nanoparticles (MSNPs–PMAT-BAE–COOH) was synthesized by the growth of PTBAEMA via surface-initiated atom-transfer radical polymerization, then reacted with succinic anhydride reaction. The chemical structure of MSNPs–PMATBAE–COOH was confirmed using multiple methods, including FT-IR and DLS, and the core-brush morphology was observed clearly using TEM. MSNPs–PMATBAE–COOH were subsequently employed to adsorb hazardous dyes efficiently. The anionic polymer brushes enabled the adsorption of methylene blue (MB) and tetraethylrhodamine (TER) at optimum pH value of 3. The results also indicated that MSNPs–PMATBAE–COOH possessed significant adsorption capacity (263.4 and 212.9 mg g^{-1} for MB and TER, respectively) and fast adsorption rate (within 15 min), which can be explained by the abundance of adsorptive polymer brushes and the small size of the nanoparticles. Overall, the findings indicate that MSNPs-PMATBAE-COOH is a highly effective adsorbent material for eliminating dye pollutants from wastewater.

1. Introduction

Colorants are widely used in various manufacturing processes, such as plastic, paper, textile and food industries, and the wastewater generated by these industries often contains dyes [1]. Among different types of organic dyes, ionic dyes are the most common [1, 2]. However, ionic dyes are highly toxic and poorly biodegradable, making them difficult to remove from wastewater [3,4]. Cationic and anionic dyes are normally used in production processes due to their high miscibility in water and strong affinity towards products

like textiles [5–7]. Methylene blue (MB) and tetraethylrhodamine (TER) been found to cause nausea, vomiting, diarrhea, and cancer [8–11]. Therefore, it is crucial to remove such dyes from wastewater to prevent contamination. Adsorption techniques are simple, safe, and cost-effective in treating dye-containing wastewater [12,13]. Numerous adsorbent materials have been fabricated and used for the treatment of polluted water, such as: carbon materials [14], organo-vermiculites [15], hydrogels [16], biomass materials [17], polymer resins [18], silica nanosheets [19] and mesoporous silica nanoparticles (MSNPs) [20].

MSNPs are widely used due to their controllable structures and tunable pore architecture [21]. They have been utilized as excellent carriers in various applications, including medicine [22], catalysis [23], sensors [24], chromatography [25], and adsorption [21]. Surface modification via silylation reaction is commonly required to achieve these applications [26]. However, the functional groups are often limited in their grafting density. Surface modification with polymers is commonly used in chromatographic stationary phase [27], biomedical materials [28], and adsorption [29]. There are two main ways to modify these materials: grafting to and grafting from. Grafting to the surface involves growing the polymeric chains in solution and then attaching them to the surface. However, due to steric hindrance, it is often difficult to achieve high grafting density polymer brushes using this technique. In contrast, the grafting from approach can achieve high-density polymer brushes, when the polymerization is directly initiated from the functionalized surface. This approach has become increasingly popular due to its ability to achieve controlled polymerization and produce well-defined structures [30–33]. Recently, surface-initiated atom transfer radical polymerization (SI-ATRP) has emerged as a particularly promising method for surface modification. Jing et al. described the fabrication of magnetic nanoparticles with poly (2, 3-epoxypropyl methacrylate) brushes attached to lysine molecules, which were effective in removing MB and lemon yellow (LY) dyes from contaminated water [34]. Their study demonstrated that the Lys-PGMA nanocomposite had a high adsorption capacity for these dyes, with values of 0.85 and 0.54 mmol g^{-1} for MB and LY, respectively. Magnetic MSNPs modified with poly (2-methacryloyloxy) ethyl] trimethylammonium chloride brushes, have been utilized to remove bromothymol blue (BT)and methyl orange (MO) dyes from contaminated water [35]. The nanoadsorbents exhibited high adsorption capacities, with maximum values of 344 mg g^{-1} for BT and 547,344 mg g^{-1} for MO. Quaternized poly (2-(N,N -diethylamino)ethyl methacrylate) with 2-iodoethanol grafted onto magnetic MSNPs was used as a nanoadsorbent to remove sunset yellow and MO dyes from polluted water with maximum adsorption capacities of MO and sunset yellow of ca. 294 mg g^{-1} and ca. 195 mg g^{-1}, respectively [36]. Poly methacrylic acid 2-(tert-butylamino)ethyl ester brushes grafted onto MSNPs surface have been employed to remove paracetamol and chlorophenoxy herbicides from polluted water [37,38]. The nanomaterials exhibited high performance in removing the contaminants, with maximum adsorption capacities of approximately 237 mg g^{-1} and 290 mg g^{-1} for paracetamol and chlorophenoxy herbicides, respectively.

Carboxylic acid groups on the adsorbent material play important role for effective dye removal. These functional groups can enhance the adsorption capacity, allowing for increased removal efficiency. The adsorption behavior of carboxylic acid groups is influenced by pH, optimizing their performance for different dye molecules. Additionally, these groups can form coordination complexes with metal ions, aiding in the removal of metal-complexed dyes. Therefore, the aim of the study was to synthesize MSNPs functionalized with poly (methacrylic acid 2-(tert-butylamino)ethyl ester brushes and modified with carboxylic acid groups in their repeating unit (MSNPs–PMATBAE–COOH). The proposed hybrid nanoparticles consist of carboxylic acid groups in their repeating units, along with hydrophobic groups attached to polymeric segments. These multifunctional materials have unique advantages for removing various toxic elements and organic molecules from contaminated water. The modified nanomaterials were fully characterized using several techniques, including TEM, FT-IR, and DLS. MSNPs–PMATBAE–COOH were utilized as an adsorbent to remove MB and TER. The effects of pH, contact time and concentration on the adsorption were explored using batch methods. To determine the adsorption mechanisms, isotherms and kinetic models were applied on the adsorption data.

2. Experimental method

2.1. Materials and instruments

Tetraethylrhodamine (TER, 97 %), methylene blue (MB, ≥95 %), 3-aminopropyltriethoxysilane (APTES, ≥98 %), α-bromoisobutyryl bromide (BIBB, 98 %), dichloromethane (DCM, ≥99.8 %), ammonium hydroxide (32 wt%), ethanol (≥99.8 %), ammonium chloride (≥99.5 %), triethylamine (≥99.5 %), n-hexane (≥95 %), 2,2′-bipyridyl (Bipy, ≥99 %), methacrylic acid 2-(tert-butylamino) ethyl ester (TMABAE, 97 %), copper (II) bromide (CuBr$_2$, ≥99 %), N-cetyltrimethylammonium bromide (CTAB, ≥98 %), methanol (≥99.9 %) and copper(I) chloride (CuCl, ≥99 %) were received from Sigma-Aldrich. Isopropanol (IPA, ≥99.5 %), hydrochloric acid (37 %), pyridine (≥99 %) and hydrogen peroxide (30 %) were received from Fisher Scientific. Tetraethyl orthosilicate (TEOS, >98 %) was received from Tokyo Chemical Industry (TCI). All chemicals were used as received.

The pH of the solution was adjusted using two solutions of 0.01 mol/L HCl and 0.05 mol/L NaOH, and measured with a pH meter (Adwa Instruments 1000 CE). The dye's concentration was determined from standard curve (R^2 = 0.994) from the absorbance obtained from a UV/vis spectrophotometer (Shimadzu instrument, UV-2600). Transmission electron microscope (TEM, JEOL instrument, JEM-1230) was used to characterize he morphology and pore structure of the particles. The surface zeta potential of the particles was determined at 25 °C using dynamic light scattering (Malvern instrument, Zetasizer Nano ZS). The presence of organic functional groups on the particle's surface was confirmed using a Fourier transform infrared spectrometer (Thermo Scientific Nicolet, iS10), in the spectral range of 4000–400 cm^{-1}.

2.2. Preparation of adsorbent

2.2.1. Preparation of MSNPs

The process for preparing MSNPs was conducted using the same method reported in previous studies [39,40]. In this process, ammonium hydroxide (9 mL) and CTAB (1 g) were dissolved in distilled water (150 mL) and heated for 20 min at 38 °C while being stirred. A mixture of TEOS (20 mL) and n-hexane (5 mL) was then added slowly, and the resulting solution was left to stir overnight at 38 °C. After centrifuging the solution, a white solid product was obtained, which was then washed with distilled water and methanol and dried in an oven at 90 °C for 3 h.

To create CTAB free MSNPs, the resulting white solid nanoparticles were dispersed in a solution of ammonium chloride in methanol (1 g/100 mL), and sonicated at 60 °C for 3 h. The final product was washed with distilled water and methanol and dried in an oven at 80 °C for 3 h.

2.2.2. ATRP initiator coated MSNPs (MSNPs–initiated)

Initially, the CTAB free MSNPs were made reactive by attaching amine groups onto the surface. This was accomplished by dispersing 0.5 g of the CTAB free MSNPs in 60 mL of toluene using ultrasound and then, adding 0.2 mL of APTES to the suspension, which was then heated overnight at 125 °C. The resulting product was a white solid, which was obtained by centrifugation for 15 min at 6000 rpm. The solid was then washed five times with distilled water and ethanol, and dried in an oven at 80 °C for 3 h.

Next, the amine-functionalized MSNPs were suspended in 30 mL of DCM using ultrasound. To this mixture, 0.2 mL of BIBB and 0.3 mL of triethylamine were added and stirred 14 h at 25 °C. The solid product was obtained by centrifugation for 15 min at 6000 rpm, and was washed five times with DCM and ethanol. MSNPs–initiated were then dried in an oven at 80 °C for 3 h.

2.2.3. PMATBAE brushes grafted onto MSNP surface

To prepare MSNPs–PMATBAE, 0.5 g of MSNPs–initiated was dispersed in 1 mL of distilled water, 4 mL of IPA, and TBAEMA weighing 2.5 g. The mixture was deoxygenated for 25 min at 40 °C. $CuBr_2$ weighing 0.002 g and Bipy weighing 0.03 g were then added to the mixture and allowed to deoxygenate for 20 min. Next, 0.002 g of CuCl was added to the polymerization solution and left to proceed at 40 °C under nitrogen atmosphere for 3 h. MSNPs–PMATBAE were washed five times with distilled water and ethanol, and the nanoparticles were dried in an oven at 80 °C for 3 h.

2.2.4. Carboxylic functionalized PMATBAE brushes

A sample of MSNPs–PMATBAEweighing 1.5 g was suspended in a mixture of DCM (5 mL) and pyridine (5 mL). Then, 0.05 g of succinic anhydride was added to the mixture, which was then sonicated for 30 min. The suspension was stirred overnight room temperature. MSNPs–PMATBAE–COOH were separated and washed five times with DCM and ethanol and the nanoparticles were dried in an oven at 80 °C for 3 h.

2.3. Batch method

Initially, dye stock solutions were created by dissolving specific quantities in distilled water, adjusting the pH with solution of HCl and 0.01 M NaOH. To assess MB and TER removal efficiency using the MSNPs–PMATBAE–COOH, 0.01 g of nanomaterial was added to a 15 mL sample tube containing 10 mL of the designated dye concentration. Next, the sample tube was sonicated for 15 s to disperse the adsorbent. Then, the tube was placed in a shaker at 200 rpm. The solution was separated using a centrifuge at 6000 rpm for 5 min, followed by a second centrifugation of the top layer at 14,000 rpm for 5 min. The remaining dye concentration was calculated from the absorbance of solution obtained from a UV/Vis spectrophotometer.

The removal efficiency was calculated by: $\% = (C_0–C_e)/C_0 \times 100\,\%$, where the initial and equilibrium concentrations of dyes in the solution were denoted by C_o (mg•L^{-1}) and C_e (mg•L^{-1}), respectively. Equation $q_e = (C_0–C_e)V/m$ was applied to determine the adsorption equilibrium capacity (q_e) in mg•g^{-1}, where V stands for the solution volume in L and m stands for the mass of MSNPs–PMATBAE–COOH in g.

2.3.1. Adsorption isotherms

Adsorption isotherms are mathematical models that illustrate the connection between the adsorbate concentration in a solution and the quantity of adsorbate molecules that bind to a surface at a constant temperature. The Langmuir isotherm is widely employed for monolayer adsorption on a uniform surface and proposes that adsorption happens at specified sites with finite capacity. The Langmuir equation is presented by $q_e = q_m K_L C_e/(1 + K_L C_e)$, where q_e is the amount of adsorbate that attaches to a unit mass of adsorbent, q_m denotes the maximum adsorption capacity, K_L signifies the Langmuir constant associated with the adsorption energy, and C_e is the equilibrium concentration of the adsorbate in the solution. The Freundlich isotherm is a model that accommodates multilayer adsorption and uneven surface environments. The Freundlich equation is articulated as $q_e = K_f \times C_e^{1/n}$, where n and K_f are the Freundlich constants connected to strength and adsorption capacity and, respectively. The Temkin isotherm is an intermediary model that considers the effect of both the interaction energy between the adsorbent and adsorbate, and the interaction energy among adsorbate molecules. The Temkin equation is described as $q_e = Bln\,(AT) + Bln\,(KT)$, where q_e is the amount of adsorbate that binds to a unit mass of adsorbent, B represents the Temkin constant related to heat of adsorption, A denotes the Temkin isotherm constant, T represents the temperature, and K signifies the equilibrium constant.

2.3.2. Kinetic studies

Kinetic models are mathematical models that describe the rate and mechanisms of adsorption. The pseudo-first-order model is a commonly used model that assumes that the rate of adsorption is proportional to the number of available adsorption sites. Its equation is $\ln(q_e - q_t) = \ln q_e - (k_1/2.303)t$, where q_e and q_t represent the amounts of adsorbate adsorbed at time t and equilibrium, respectively. The rate constant of the pseudo-first-order model is k_1 and t denotes the time. The pseudo-second-order model is used model that considers chemisorption and assumes that the rate of adsorption is proportional to the square of the number of available adsorption sites. Its equation is $t/(q_t) = 1/(k_2 \, q_e^2) + t/q_e$, where k_2 is the rate constant of the pseudo-second-order model. The intraparticle diffusion is commonly used model to identify the rate-limiting step of adsorption and assumes that adsorption happens in multiple stages, including external transport, boundary layer diffusion, and intraparticle diffusion. Its equation is $q_t = k_i t^{0.5} + C$, where C is the intercept that considers the effects of the boundary layer and k_i is the intraparticle diffusion rate constant.

## 3. Results and discussion

3.1. Characterization of nanomaterials

Scheme 1 demonstrates the synthesis process for the MSNPs–PMATBAE–COOH. First, MSNPs were formed through the condensation of TEOS under basic conditions, with CTAB as the template and n-hexane as porous expander. MSNPs' surfaces were functionalized with amine groups using APTES through a post-grafting technique. The organic functional groups containing amine groups were covalently attached to "Si–OH" groups on both the external and internal surfaces of MSNPs. Amine groups were then able to react quickly with BIBB molecules, resulting in ATRP initiator layers on MSNPs' surfaces. The surface-initiated atom transfer radical polymerization (SI-ATRP) method was employed to grow uniform PMATBAE brushes on MSNPs' surfaces. Succinic anhydride was used to generate carboxylic acid groups on polymer chains after reacting with the secondary amine in PMATBAE segments. The nanomaterials were characterized comprehensively using techniques such as FT-IR, DLS, and TEM.

Transmission electron microscopy (TEM) is a powerful imaging technique that is usually utilized to study the physical properties and morphology of materials at the nanoscale. Thus, the physical structure of MSNPs–initiated, MSNPs–PMATBAE, and MSNPs–PMATBAE–COOH was examined using TEM. Fig. 1A–C reveal that the nanoparticles all had an average diameter in the range of 100–340 nm, and possessed an ordered pore structure with a hexagonal array. The average radius of the pores was approximately 5 nm. This pore structure is what gives these nanoparticles their unique properties, as it allows them to be applied in environmental remediation. The polymerization process was successful, as evidenced by the blurry appearance of the pores after polymer brush immobilization.

The FT-IR analysis was utilized to confirm the chemical composition changes that occurred during the fabrication of the particles. Fig. 2 shows the FT-IR spectra of the MSNPs–initiated, MSNPs–PMATBAE and MSNPs–PMATBAE–COOH, with scanning performed in the 400–4000 cm^{-1} range. The spectra revealed peaks corresponding to Si–O–Si bending and Si–OH stretching at approximately 450, 800, 1080, and 3400 cm^{-1}. A peak at ~1640 cm^{-1} could be implied to the presence of water molecules physiosorbed on the nanoparticle surfaces. The FT-IR spectra of MSNPs–initiated exhibited peaks at ~1440 and ~2950 cm^{-1}, attributed to –CH$_2$– stretching vibrations. After ATRP polymerization, new peaks appeared at ~1450 and ~1730 cm^{-1}, corresponding to CH$_2$ bending and C=O, respectively. Additionally, the peak intensity of C–H stretching increased at 2930 cm^{-1}. While no significant changes were observed in the FT-IR spectra after the reaction with succinic anhydride, except the appearance of a new peak at~1570 cm^{-1}, provided evidence of the successful reaction between secondary amine succinic anhydride to generate carboxylic acid.

Fig. 3 displays the variations in zeta potentials (ζ) of MSNPs–initiated, MSNPs–PMATBAE and MSNPs–PMATBAE–COOH as a function of pH. For MSNPs–initiated, the zeta potential value remained almost neutral, with a range of 6 to −11 mV across the selected pH values. MSNPs–PMATBAE sample was positively charged at pH values below the pKa of PMATBAE with zeta potential values ranged from 18 to 35 mV, due to the protonation of secondary amines. Above the pKa, the zeta potential became nearly neutral, with values ranging from 10 to 5 mV. MSNPs–PMATBAE–COOH had a negative zeta potential, which decreased gradually from −22 to −38 mV at pH values ranging from 4 to 9. This decrease in zeta potential is attributed to the deprotonation of carboxylic acid groups existing in the PMATBAE-COOH coating on the MSNPs.
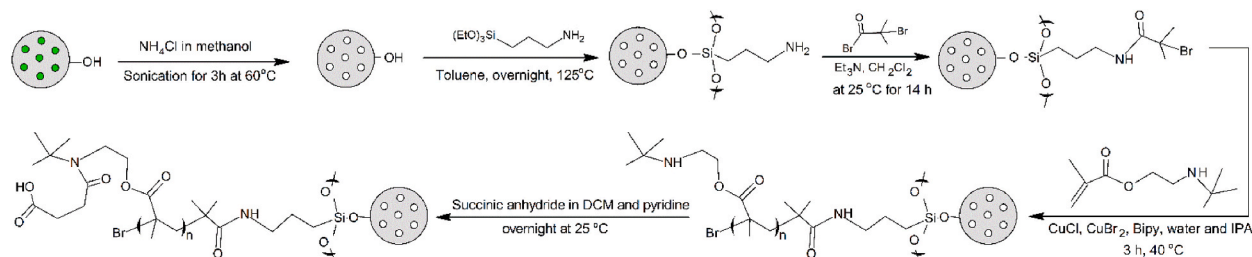
Scheme 1. Shows the process used to fabricate the MSNPs–PMATBAE–COOH, with a simplified visual representation of the steps involved in their fabrication.
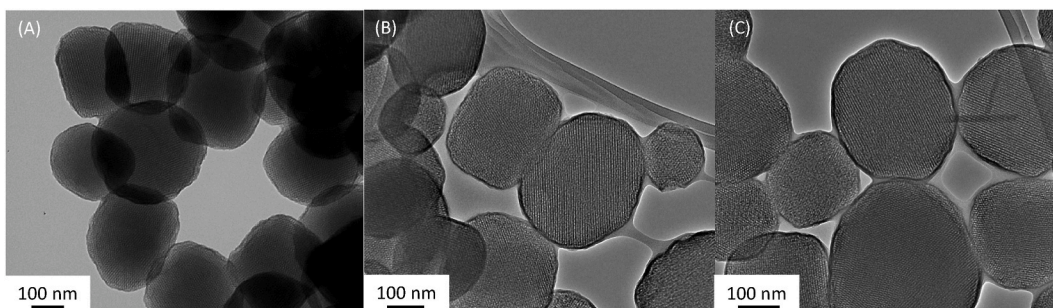
Fig. 1. TEM images reveal the topological structures of the fabricated nanoparticles: A) MSNPs–initiated, B) MSNPs–PMATBAE, and C) MSNPs–PMATBAE–COOH.
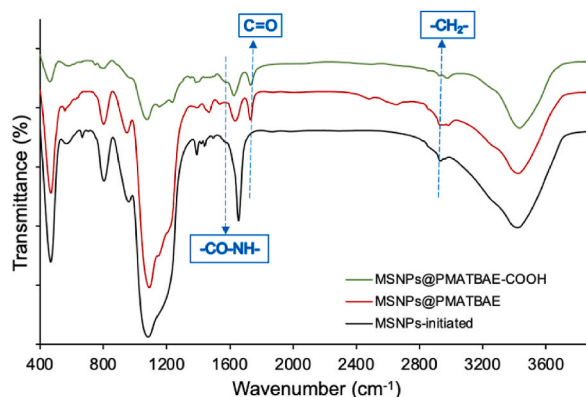

Fig. 2. FT-IR spectra of the surface modified MSNPs: (black) MSNPs–initiated, (red) MSNPs–PMATBAE and (green) MSNPs–PMATBAE–COOH. (For interpretation of the references to colour in this figure legend, the reader is referred to the Web version of this article.)
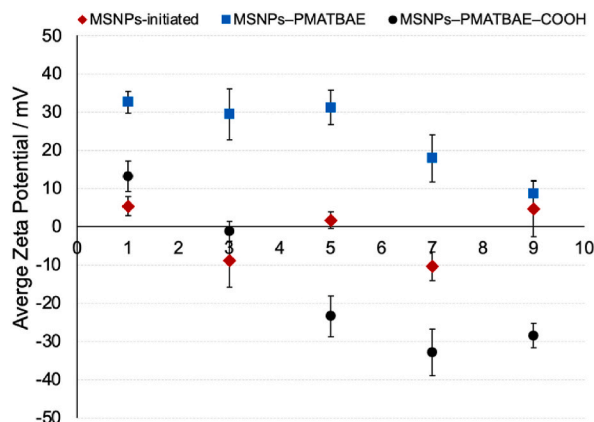

Fig. 3. Zeta potential of the surface modified MSNPs: (rhombus) MSNPs–initiated, (square) MSNPs–PMATBAE and (circle) MSNPs–PMAT-BAE–COOH, obtained from aqueous solutions at different values of pH.

3.2. Batch adsorption studies

3.2.1. Effect of pH solution and concentrations of dyes

The solution's pH is one of the main variables that could impact the adsorption efficiency of the sorbent. The pH range between 1 and 9 was selected to examine the dye's adsorption patterns on MSNPs–PMATBAE–COOH. Scheme 2 presents the chemical structures of TER and MB. At ambient temperature, the amount of TER and MB adsorbed onto the sorbent at different pH and initial concentrations are presented in Fig. 4. The results show that the optimum pH value for TER was to be somewhere between pH 1 and 3, whereas the optimum pH value for MB was to be somewhere between pH 1 and 5, Fig. 4A. The inclusion of carboxylic acid groups gives
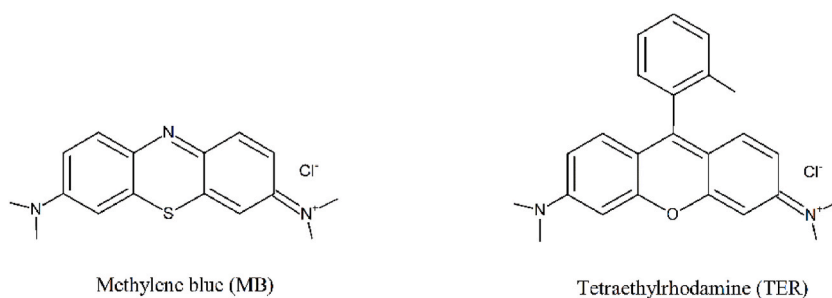
Scheme 2. Representation the chemical structures of dyes used in this study.
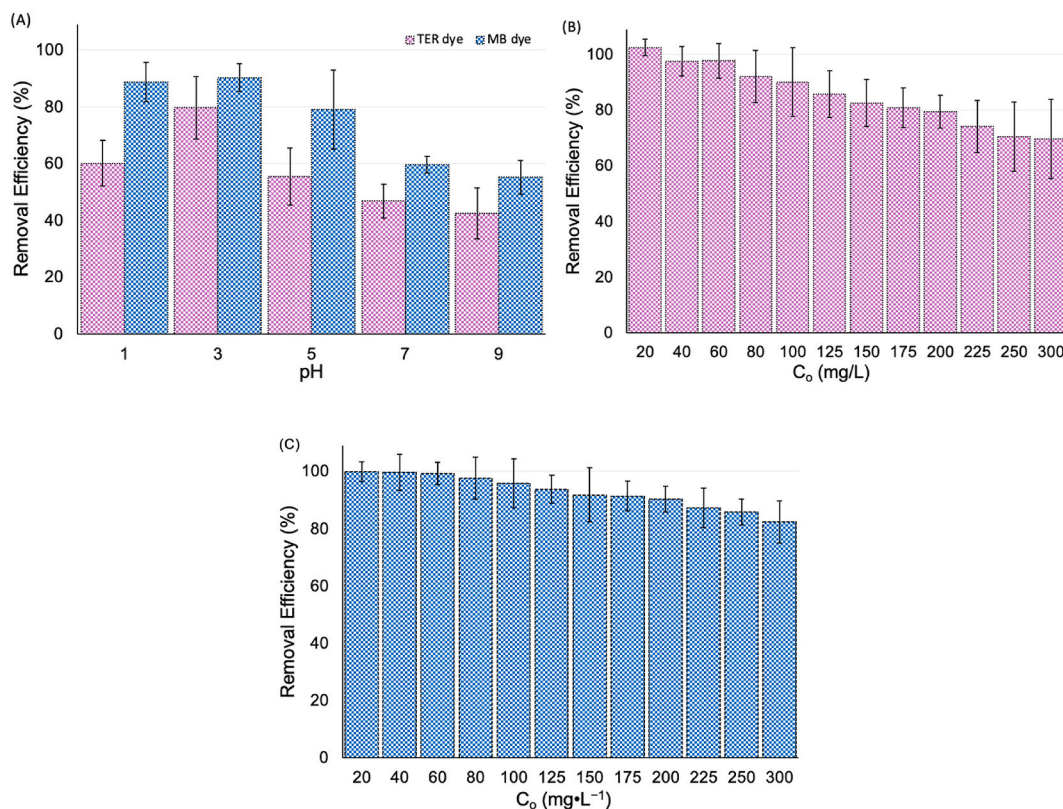

Fig. 4. (A) The effect of pH on the dyes uptake from contaminated water by 10 mg of MSNPs–PMATBAE–COOH at 25 °C, 200 rpm and 150 min contact time. (B) and (C) The effect of initial concentration of TER and MB, respectively, on the dye's uptake from an aqueous solution by 10 mg of MSNPs–PMATBAE–COOH at pH 3, 298 K, 200 rpm and 120 min contact time.

the adsorbent an anionic character at pH above 3, with a zeta potential value of around −34 mV. The MSNPs–PMATBAE–COOH were neutral character, with a zeta potential value between +13 and −11 mV at a pH below 3. TER dye has a zwitterionic character at pH 5–6, and cationic character at pH below 4. MB dye has a cationic character at pH below 6. The highest adsorption capacities of both dyes were in acidic media, which might be explained by electrostatic interaction between the surfaces of MSNPs–PMATBAE–COOH and the dyes.

To comprehend the effect of the initial concentration on the decontamination efficiency, a wide variety of dye concentrations were applied. As illustrated in Fig. 4C and D, MSNPs–PMATBAE–COOH (0.01 g) at 25 °C were suspended in a variety of dye's concentrations between 20 and 300 ppm. The adsorption capacity trended increasing as the dye concentration increased. The active sites of MSNPs–PMATBAE–COOH were largely empty at low concentrations. The number of dyes' molecule increased as the concentration rose until the active sites of the adsorbent were saturated. When all active sites of the adsorbent had been occupied, the removal efficiency dropped at increasing concentrations.

3.2.2. Adsorption isotherms

Adsorption isotherm models are typically applied to analyze surface characteristics, capacities, and adsorbent affinities. Plotting the amount of analyte absorbed per unit mass of the sorbent against the equilibrium concentration of the adsorbent allowed the isotherm models to be presented. Three isotherm models: Langmuir, Freundlich and Temkin were used in this study to fit the experimental data. The sorption isotherms that are most frequently utilized are these theoretical models. The Langmuir isotherm characterizes the equilibrium between the amount of analytes adsorbed on the sorbent and the excess amount of analyte present in the solution at a constant temperature. As long as there were active sites available, the number of analyte adsorbed increased as the concentration of the analyte rose. The quantity of analyte adsorbed on the surface of the sorbent did not change with concentration when all the active sites of the sorbent were occupied by the analyte.

The slope and intercept of the linear plots were used to calculate the relative parameters of the selected adsorption isotherms models. Good correlation coefficient values ($R^2 > 0.96$) showed that the models of Freundlich and Langmuir fit the experimental data with an acceptable manner. The Langmuir model seems to provide a better description of both MB and TER onto MSNPs–PMAT-BAE–COOH than the Freundlich model, as indicated by correlation coefficients, Fig. 5 and Table 1. It suggested that one layer of the adsorbate molecules is uniformly and homogeneously formed on the surface.

3.2.3. Kinetic studies

Kinetic investigations offer insights into the characteristics and rate of adsorption and desorption in adsorption processes. These reactions rely on time, making it crucial to show the adsorption and desorption rates for the development of adsorbents and evaluation of the adsorption and desorption processes. Theoretical models, pseudo-first-order, pseudo-second-order, and intraparticle diffusion, have been employed to elucidate the nature of these adsorption reactions. The adsorption data for MB and TER on the MSNPs–PMATBAE–COOH were analyzed using linear forms of the pseudo first-order, pseudo second-order, and intraparticle diffusion
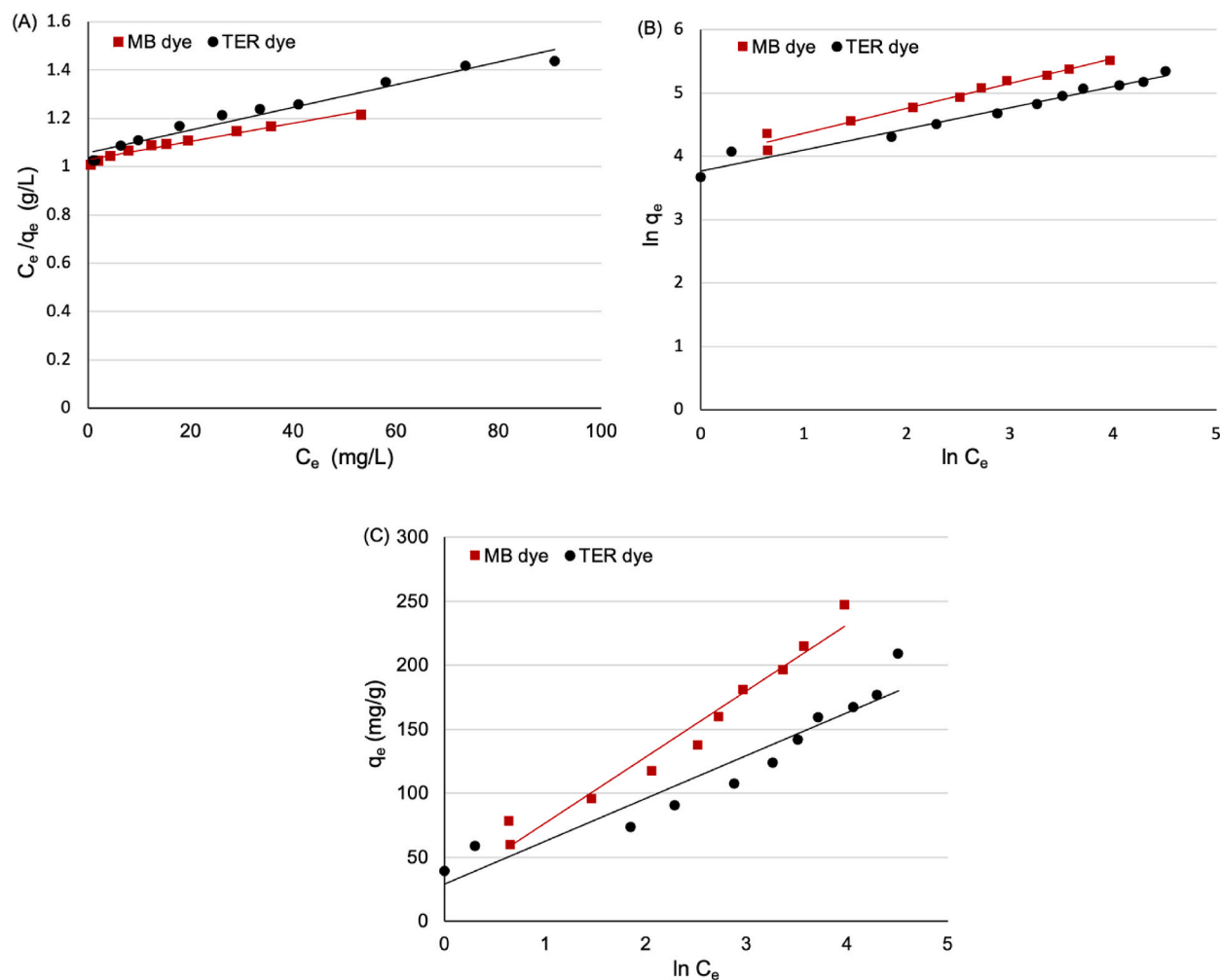

Fig. 5. The adsorption experimental data fitted to linear isotherm models: (A) Langmuir isotherm, (B) Freundlich isotherm and (C) Temkin isotherm. Conditions: 10 mg of MSNPs–PMATBAE–COOH at pH 3, 298 K, 200 rpm and 120 min contact time.

Table 1
Langmuir, Freundlich and Temkin isotherms constants for adsorption of MB and TER on 10 mg of MSNPs–PMATBAE–COOH at pH 3, 298 K, 200 rpm and 120 min contact time.

MB	Langmuir isotherm	q_{max} (mg•g^{-1})	263.49
		K_L (L•mg^{-1})	0.00368
		R_L	0.47465–0.93128
		R^2	0.97576
	Freundlich isotherm	n (L•mg^{-1})	2.56
		K (mg•g^{-1})	53.25
		R^2	0.96672
	Temkin isotherm	A (L•g^{-1})	1.63
		R^2	0.96304
TER	Langmuir isotherm	q_{max} (mg•g^{-1})	212.97
		K_L (L•mg^{-1})	0.00444
		R_L	0.42873–0.91841
		R^2	0.97167
	Freundlich isotherm	n (L•mg^{-1})	2.99
		K (mg•g^{-1})	43.29
		R^2	0.96214
	Temkin isotherm	A (L•g^{-1})	2.28
		R^2	0.91374

models. Fig. 6 illustrations the results of the analysis. In pseudo first-order, a graph of log (q_e-q_t) versus t was plotted with slope equal to $k_1/2.303$ and intercept equal to logq_e. The adsorption rate constants were presented in Table 2 along with the values of R^2 and the estimated $q_{e,cal}$ values. However, the R^2 for the first-order model was not high, and the estimated $q_{e,cal}$ values from the model did not fit with the experimental data, indicating that the model is not suitable for describing these processes. When a graph of t/q_t versus t was plotted, it resulted in a straight line with a slope of $1/q_e$ and an intercept of $1/k_2q_e^2$. The values of k_2 and q_e along with their R^2 values were shown in Table 2. The R^2 of MB and TER were close to 1 (0.99 and 0.98, respectively) and the calculated $q_{e,cal}$ values were close to the experimentally obtained $q_{e,exp}$ values, indicating that the adsorption processes of both dyes followed a pseudo-second-order kinetic model.

In the graph displaying q_t against the square root of time ($t^{1/2}$), the intraparticle diffusion model reveals three distinct slopes for both MB and TER adsorption (Fig. 6C). This indicates that the adsorption events transpire through a multi-stage approach [41]. The adsorption of MB onto MSNPs–PMATBAE–COOH showed a high rate during the initial 15 min, after which the rate progressively slowed down. After 50 min, the sorbent surface was saturated. The removal of TER from the solution using the adsorbent exhibited a similar adsorption pattern. The first step of the process was attributed to both macro-pore and boundary-layer diffusion, while the second step was related to micro-pore and intraparticle diffusion.

3.2.4. Regeneration and desorption studies

When creating an affordable water treatment process, it is crucial to consider the regeneration of the adsorbents as a significant factor. The used MSNPs–PMATBAE–COOH were restored using eluents like diluted hydrochloric acid and diluted sodium hydroxide and ethanol. The ability of the regenerated MSNPs–PMATBAE–COOH to remove the dyes at 100 mg/L was tested over three cycles, and the adsorption capacity decreased from 94 % to 70 %, as shown in Fig. 7. This suggests that the MSNPs–PMATBAE–COOH adsorbent has the potential to be beneficial in environmental applications because it maintained high reusability even after being regenerated four times.

Table 3 presents the elemental analysis data for the adsorbent before and after conducting the experiments. The initial as-made MSNPs–PMATBAE–COOH adsorbent exhibited carbon (C) content of 19.74 %, hydrogen (H) content of 3.61 %, nitrogen (N) content of 3.47 %, and sulfur (S) content of 0.03 %. After adsorbing MB and TER onto the adsorbent, the carbon, hydrogen, nitrogen, and sulfur contents increased. For MB adsorption, the respective values were 27.53 %, 4.95 %, 5.02 %, and 2.07 %, while for TER adsorption, they were 29.12 %, 5.76 %, 5.82 %, and 0.08 %. Regenerated adsorbents from MB and TER exhibited carbon, hydrogen, nitrogen, and sulfur contents of 20.11 %, 3.72 %, 3.70 %, and 0.30 %, and 21.49 %, 3.76 %, 3.82 %, and 0.06 %, respectively. These results provide insights into the elemental composition changes of the adsorbent throughout the experimental process.

4. Conclusion

In conclusion, mesoporous nanoparticles with a core-brush nanostructure (MSNPs–PMATBAE–COOH) were produced by combining surface-initiated atom-transfer radical polymerization and succinic anhydride functionalization to decontaminate ionic organic dyes efficiently. The results showed that the efficiency of the decontamination process increased with increasing contact time. However, increasing the concentration of both dyes in the solution decreased the removal efficiency. Under optimal conditions, the removal efficiency was observed at pH 3 for both dyes, likely due to the electrostatic interaction between the polymer chains and dye molecules. The adsorption of MB and TER onto the MSNPs–PMATBAE–COOH adsorbent followed equilibrium data fitted well with the Langmuir isotherm and the pseudo-second-order kinetics for both dyes. The adsorption capacity of MB and TER at equilibrium, obtained from the theoretical model, was 263.49 mg g^{-1} and 212.97 mg g^{-1}, respectively. Notably, the MSNPs–PMATBAE–COOH adsorbent demonstrated promising potential for removing organic dyes from wastewater.
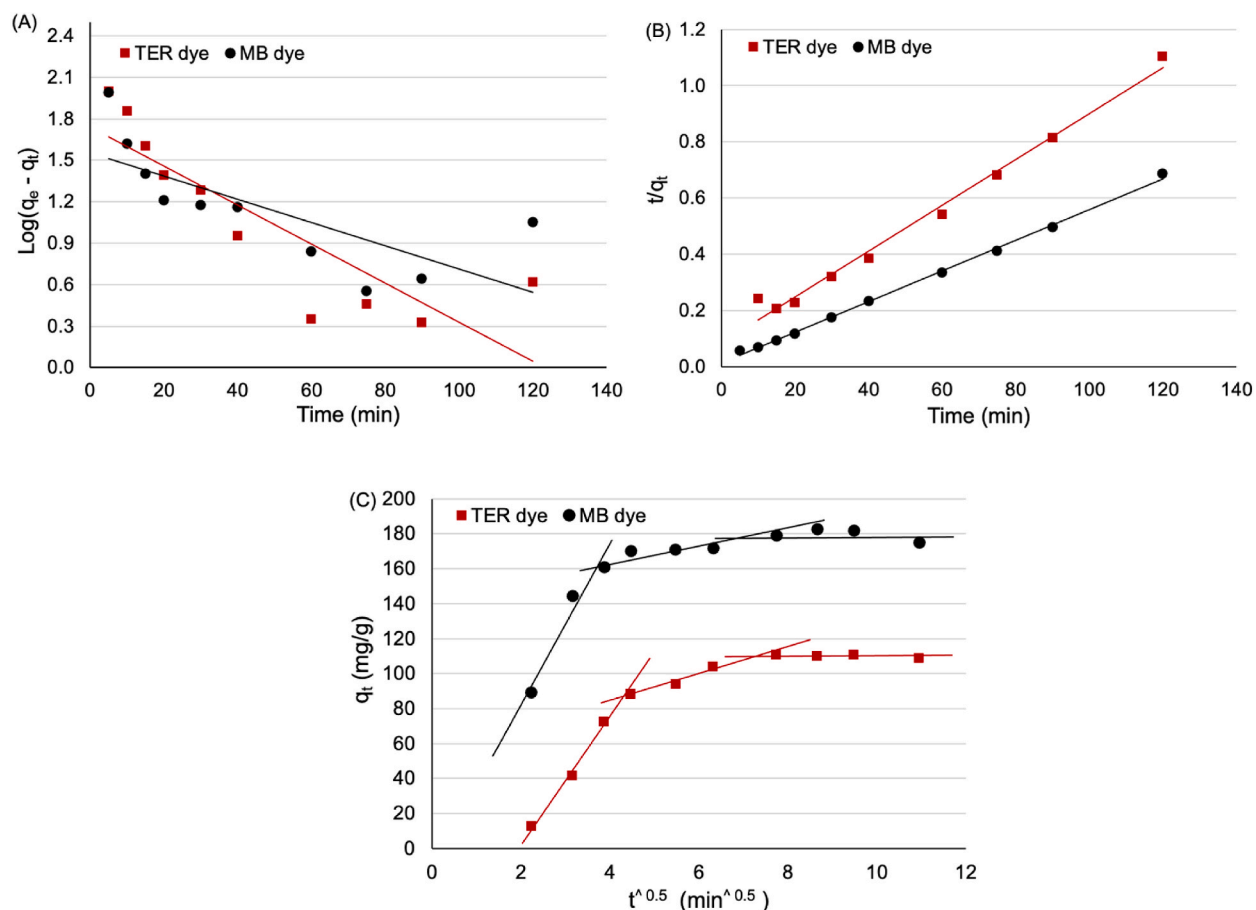
Fig. 6. The adsorption experimental data fitted to linear kinetic models: (A) pseudo-first-order, (B) pseudo-second-order and (C) intraparticle diffusion. Conditions: 10 mg of MSNPs–PMATBAE–COOH at pH 3, 25 °C and 200 rpm.

Table 2
Constant parameters of pseudo-first-order and pseudo-second-order for adsorption of MB and TER on 10 mg of MSNPs–PMAT-BAE–COOH at pH 3, 298 K and 200 rpm.

MB	Pseudo-first-order	q_e (mg•g^{-1})	4.73
		k_1 (min^{-1})	0.01941
		R^2	0.55417
	Pseudo-second-order	q_e (mg•g^{-1})	183.09
		k_2 (g.g^{-1}•min^{-1})	0.00224
		R^2	0.99786
TER	Pseudo-first-order	q_e (mg•g^{-1})	5.69
		k_1 (min^{-1})	0.03249
		R^2	0.74187
	Pseudo-second-order	q_e (mg•g^{-1})	122.59
		k_2 (g.g^{-1}•min^{-1})	0.00078
		R^2	0.98738

Data availability

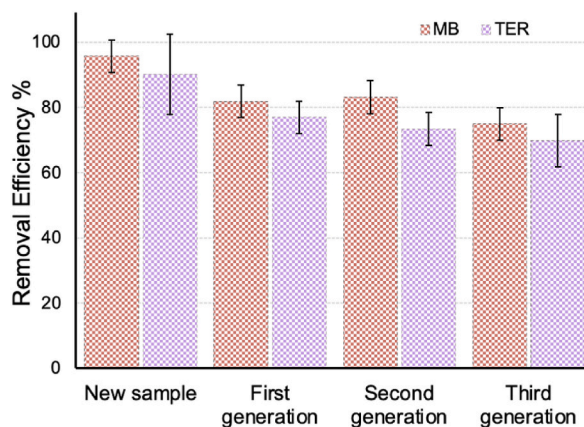Data included in article/supplementary material/referenced in article.

Fig. 7. The study on the reusability of MSNPs–PMATBAE–COOH is presented through graphs that show the results of four adsorption-reuse cycles. The adsorption was conducted using 0.1 g of the adsorbent, 100 ppm MB at pH 3, and 100 ppm TER at pH 3.

Table 3
Elemental analysis data obtained for the adsorbent before and after preforming the experiments.

MATERIALS	%C	%H	%N	%S
As made MSNPs–PMATBAE–COOH	19.74	3.61	3.47	0.03
MB onto MSNPs–PMATBAE–COOH	27.53	4.95	5.02	2.07
TER onto MSNPs–PMATBAE–COOH	29.12	5.76	5.82	0.08
Regenerated MSNPs–PMATBAE–COOH (from MB)	20.11	3.72	3.70	0.30
Regenerated MSNPs–PMATBAE–COOH (from TER)	21.49	3.76	3.82	0.06

CRediT authorship contribution statement

Abdullah Mohammed Alswieleh: Writing – review & editing, Writing – original draft, Resources, Methodology, Formal analysis, Data curation, Conceptualization.

Declaration of competing interest

The authors declare that they have no known competing financial interests or personal relationships that could have appeared to influence the work reported in this paper.

Acknowledgments

References

[1] S.H. Teo, C.H. Ng, A. Islam, G. Abdulkareem-Alsultan, C.G. Joseph, J. Janaun, Y.H. Taufiq-Yap, S. Khandaker, G.J. Islam, H. Znad, Sustainable toxic dyes removal with advanced materials for clean water production: a comprehensive review, J. Clean. Prod. 332 (2022), 130039.

[2] G. Sriram, A. Bendre, E. Mariappan, T. Altalhi, M. Kigga, Y.C. Ching, H.-Y. Jung, B. Bhaduri, M. Kurkuri, Recent trends in the application of metal-organic frameworks (MOFs) for the removal of toxic dyes and their removal mechanism-a review, Sustainable Materials and Technologies 31 (2022), e00378.

[3] A. Anderson, A. Anbarasu, R.R. Pasupuleti, M. Sekar, T. Praveenkumar, J.A. Kumar, Treatment of heavy metals containing wastewater using biodegradable adsorbents: a review of mechanism and future trends, Chemosphere (2022), 133724.

[4] A. Khan, A. Roy, S. Bhasin, T.B. Emran, A. Khusro, A. Eftekhari, O. Moradi, H. Rokni, F. Karimi, Nanomaterials: an alternative source for biodegradation of toxic dyes, Food Chem. Toxicol. (2022), 112996.

[5] P.D. Karmakar, A. Pal, Rapid and selective removal of toxic cationic dye using biodegradable copolymer derived from glycogen and poly (acrylic acid) through ATRP, J. Indian Chem. Soc. 100 (1) (2023), 100844.

[6] S.S. Qureshi, V. Shah, S. Nizamuddin, N. Mubarak, R.R. Karri, M.H. Dehghani, S. Ramesh, M. Khalid, M.E. Rahman, Microwave-assisted synthesis of carbon nanotubes for the removal of toxic cationic dyes from textile wastewater, J. Mol. Liq. 356 (2022), 119045.

[7] P. Das, S. Nisa, A. Debnath, B. Saha, Enhanced adsorptive removal of toxic anionic dye by novel magnetic polymeric nanocomposite: optimization of process parameters, J. Dispersion Sci. Technol. 43 (6) (2022) 880–895.

[8] M.A. Asbollah, M.S.M. Sahid, E.W.E. Shahrin, N.A.H. Narudin, E. Kusrini, N.N.M. Shahri, J. Hobley, A. Usman, Dynamics and thermodynamics for competitive adsorptive removal of methylene blue and rhodamine B from binary aqueous solution onto durian rind, Environ. Monit. Assess. 194 (9) (2022) 645.

[9] B. Erdem, S. Sevinç, S. Erdem, R.M. Öksüzoğlu, Comparative influence of adsorption assisted magnetic mesoporous TiO2 photocatalyst for the removal of methylene blue and rhodamine B, React. Kinet. Mech. Catal. (2023) 1–17.

[10] P.O. Oladoye, T.O. Ajiboye, E.O. Omotola, O.J. Oyewola, Methylene Blue Dye: Toxicity and Potential Technologies for Elimination from (Waste) Water, Results in Engineering, 2022, 100678.

[11] A.A. Al-Gheethi, Q.M. Azhar, P.S. Kumar, A.A. Yusuf, A.K. Al-Buriahi, R.M.S.R. Mohamed, M.M. Al-Shaibani, Sustainable approaches for removing Rhodamine B dye using agricultural waste adsorbents: a review, Chemosphere 287 (2022), 132080.

[12] R. Rashid, I. Shafiq, P. Akhter, M.J. Iqbal, M. Hussain, A state-of-the-art review on wastewater treatment techniques: the effectiveness of adsorption method, Environ. Sci. Pollut. Control Ser. 28 (2021) 9050–9066.

[13] X. Guo, J. Wang, A general kinetic model for adsorption: theoretical analysis and modeling, J. Mol. Liq. 288 (2019) 111100.

[14] C. Sarkar, C. Bora, S.K. Dolui, Selective dye adsorption by pH modulation on amine-functionalized reduced graphene oxide–carbon nanotube hybrid, Ind. Eng. Chem. Res. 53 (42) (2014) 16148–16155.

[15] F. Ding, T. Shen, Q. Zhao, X. Jin, S. Mao, M. Gao, Series of bis-morpholinium-based organo-Vts for the removal of anionic dyes, J. Mol. Liq. (2022), 119424.

[16] T. Li, Y. Ding, L. Liu, J. Liu, W. Fang, Y. Xiang, T. Li, Facile fabrication of multifunctional perfluoroalkyl functionalized graphene hydrogel via a synchronous reduction and grafting strategy, J. Mater. Chem. A 3 (43) (2015) 21744–21753.

[17] G. Zhu, X. Xing, J. Wang, X. Zhang, Effect of acid and hydrothermal treatments on the dye adsorption properties of biomass-derived activated carbon, J. Mater. Sci. 52 (13) (2017) 7664–7676.

[18] X. Zhang, A. Li, Z. Jiang, Q. Zhang, Adsorption of dyes and phenol from water on resin adsorbents: effect of adsorbate size and pore size distribution, J. Hazard. Mater. 137 (2) (2006) 1115–1122.

[19] S. Mao, T. Shen, Q. Zhao, T. Han, F. Ding, X. Jin, M. Gao, Selective capture of silver ions from aqueous solution by series of azole derivatives-functionalized silica nanosheets, Chin. J. Chem. Eng. 57 (2023) 319–328.

[20] N. Hao, H.T. Chorsi, J.X. Zhang, Hierarchical lotus leaf-like mesoporous silica material with unique bilayer and hollow sandwich-like folds: synthesis, mechanism, and applications, ACS Sustain. Chem. Eng. 5 (3) (2017) 2044–2049.

[21] J.A.S. Costa, R.A. de Jesus, D.O. Santos, J.F. Mano, L.P. Romao, C.M. Paranhos, Recent progresses in the adsorption of organic, inorganic, and gas compounds by MCM-41-based mesoporous materials, Microporous Mesoporous Mater. 291 (2020), 109698.

[22] M. Manzano, M. Vallet-Regí, Mesoporous silica nanoparticles for drug delivery, Adv. Funct. Mater. 30 (2) (2020), 1902634.

[23] A. Alfawaz, A. Alsalme, A. Alkathiri, A. Alswieleh, Surface functionalization of mesoporous silica nanoparticles with brønsted acids as a catalyst for esterificatsion reaction, J. King Saud Univ. Sci. 34 (5) (2022), 102106.

[24] A. Zhu, T. Jiao, S. Ali, Y. Xu, Q. Ouyang, Q. Chen, SERS sensors based on aptamer-gated mesoporous silica nanoparticles for quantitative detection of staphylococcus aureus with signal molecular release, Anal. Chem. 93 (28) (2021) 9788–9796.

[25] J.-P. Fan, T.-T. Yuan, X.-K. Xu, X.-H. Zhang, Y.-T. Cheng, J.-J. Luo, Preparation and characterization of mock strawberry-like aminopropyl-modified mesoporous silica for column chromatographic purification of paclitaxel in Taxus× Media, Chem. Eng. J. 359 (2019) 1509–1517.

[26] R. Soltani, A. Marjani, S. Shirazian, Facile one-pot synthesis of thiol-functionalized mesoporous silica submicrospheres for Tl (I) adsorption: isotherm, kinetic and thermodynamic studies, J. Hazard Mater. 371 (2019) 146–155.

[27] A.L. Santos, G.O. Carvalho, A.M. Faria, Per-aqueous liquid chromatography stationary phase with poly (ethylene oxide-co-dimethylsiloxane) immobilized on mesoporous aluminized silica support, Microporous Mesoporous Mater. (2023), 112608.

[28] A.M. Beagan, A.A. Alghamdi, S.S. Lahmadi, M.A. Halwani, M.S. Almeataq, A.N. Alhazaa, K.M. Alotaibi, A.M. Alswieleh, Folic acid-terminated poly (2-diethyl amino ethyl methacrylate) brush-gated magnetic mesoporous nanoparticles as a smart drug delivery system, Polymers 13 (1) (2020) 59.

[29] A.M. Alswieleh, Zwitterionic polymer brushes coated with mesoporous silica nanoparticles as efficient adsorbents for dye removal from aqueous solutions, ACS Appl. Polym. Mater. 5 (2) (2023) 1334–1343.

[30] W.J. Brittain, S. Minko, A structural definition of polymer brushes, J. Polym. Sci. Polym. Chem. 45 (16) (2007) 3505–3512.

[31] S.T. Milner, Polymer brushes, Science 251 (4996) (1991) 905–914.

[32] G.C. Ritsema van Eck, L. Chiappisi, S. De Beer, Fundamentals and applications of polymer brushes in air, ACS Appl. Polym. Mater. 4 (5) (2022) 3062–3087.

[33] A.M. Bhayo, Y. Yang, X. He, Polymer brushes: synthesis, characterization, properties and applications, Prog. Mater. Sci. (2022), 101000.

[34] S. Jing, X. Wang, Y. Tan, Preparation of lysine-decorated polymer-brush-grafted magnetic nanocomposite for the efficient and selective adsorption of organic dye, Appl. Surf. Sci. 441 (2018) 654–662.

[35] A. Beagan, R. Alshammari, L. Alotaibi, H. Albarrak, K. Alotaibi, A. Alswieleh, High-Efficient anionic dyes removal from water by cationic polymer brush functionalized magnetic mesoporous silica nanoparticles, Processes 10 (8) (2022) 1565.

[36] K.M. Alotaibi, A.A. Almethen, A.M. Beagan, H.M. Al-Swaidan, A. Ahmad, S.A. Bhawani, A.M. Alswieleh, Quaternization of poly (2-diethyl aminoethyl methacrylate) brush-grafted magnetic mesoporous nanoparticles using 2-Iodoethanol for removing anionic dyes, Appl. Sci. 11 (21) (2021) 10451.

[37] K.M. Alotaibi, Mesoporous silica nanoparticles modified with stimuli-responsive polymer brush as an efficient adsorbent for chlorophenoxy herbicides removal from contaminated water, Int. J. Environ. Anal. Chem. (2021) 1–14.

[38] L.H.K. Alfhaid, Adsorption of paracetamol in contaminated water through pH-responsive polymer-brush-grafted mesoporous silica nanoparticles, Int. J. Environ. Anal. Chem. (2022) 1–17.

[39] A.M. Alswieleh, M.M. Alshahrani, K.E. Alzahrani, H.S. Alghamdi, A.A. Niazy, A.S. Alsilme, A.M. Beagan, B.M. Alsheheri, A.A. Alghamdi, M.S. Almeataq, Surface modification of pH-responsive poly (2-(tert-butylamino) ethyl methacrylate) brushes grafted on mesoporous silica nanoparticles, Des. Monomers Polym. 22 (1) (2019) 226–235.

[40] A.M. Alswieleh, A.M. Beagan, B.M. Alsheheri, K.M. Alotaibi, M.D. Alharthi, M.S. Almeataq, Hybrid mesoporous silica nanoparticles grafted with 2-(tert-butylamino) ethyl methacrylate-b-poly (ethylene glycol) methyl ether methacrylate diblock brushes as drug nanocarrier, Molecules 25 (1) (2020) 195.

[41] N.Y. Mezenner, A. Bensmaili, Kinetics and thermodynamic study of phosphate adsorption on iron hydroxide-eggshell waste, Chem. Eng. J. 147 (2–3) (2009) 87–96.